Renewable and Sustainable Energy Reviews 26 (2013) 437–445

Contents lists available at SciVerse ScienceDirect

Renewable and Sustainable Energy Reviews

journal homepage: www.elsevier.com/locate/rser

Turbulent inflow characteristics for hydrokinetic energy conversion in rivers

V.S. Neary [a,*], B. Gunawan [b], D.C. Sale [c]

[a] Sandia National Laboratories, Albuquerque, NM 87185, USA
[b] Oak Ridge National Laboratory, Oak Ridge, TN 37831, USA
[c] Mechanical Engineering Department, University of Washington, Box 352600, Seattle, WA 98195, USA

ARTICLE INFO

Article history:
Received 31 August 2012
Received in revised form
5 May 2013
Accepted 13 May 2013
Available online 2 July 2013

Keywords:
Open channel flows
Turbulence characterization
Hydrokinetic turbines
Resource assessment

ABSTRACT

Marine and hydrokinetic technologies, which convert kinetic energy from currents in open-channel flows to electricity, require inflow characteristics (e.g. mean velocity and turbulence intensity profiles) for their siting, design, and evaluation. The present study reviews mean velocity and turbulence intensity profiles reported in the literature for open-channel flows to gain a better understanding of the range of current magnitudes and longitudinal turbulence intensities that these technologies may be exposed to. We compare 47 measured vertical profiles of mean current velocity and longitudinal turbulence intensity (normalized by the shear velocity) that have been reported for medium-large rivers, a large canal, and laboratory flumes with classical models developed for turbulent flat plate boundary layer flows. The comparison suggests that a power law (with exponent, $1/a = 1/6$) and a semi-theoretical exponential decay model can be used to provide first-order approximations of the mean velocity and turbulence intensity profiles in rivers suitable for current energy conversion. Over the design life of a current energy converter, these models can be applied to examine the effects of large spatiotemporal variations of river flow depth on inflow conditions acting over the energy capture area. Significant engineering implications on current energy converter structural loads, annual energy production, and cost of energy arise due to these spatiotemporal variations in the mean velocity, turbulence intensity, hydrodynamic force, and available power over the energy capture area.

Published by Elsevier Ltd.

Contents

1. Introduction 437
2. Methods 439
3. Results and discussion 441
4. Conclusions 443
Notation 444
Acknowledgments 444
Appendix 1 Derivation of Reynolds averaged hydrodynamic force and power 444
Appendix 2 Derivation of Power Law Exponent consistent with the Manning's Equation 444
References 445

1. Introduction

The siting and design of river current energy conversion (CEC) technologies requires an assessment of the spatiotemporal variation in the current velocity and turbulence acting on the proposed energy capture area (ECA) of the CEC machine. Fig. 1 illustrates typical profiles of current velocity and turbulence intensity in open channel flows, and demonstrates how the inflow characteristics vary over the ECA of the CEC machine. The average hydrodynamic force and available power estimates over a representative period of record are calculated as

$$\overline{F} = \frac{1}{2} \times \rho \times a \times \overline{u^2} = \frac{1}{2} \times \rho \times a \times (1 + I_u^2) \times \overline{u}^2 \qquad (1)$$

* Corresponding author. Tel.: +1 865 284 2199; fax: +1 505 844 6541.
E-mail address: vsneary@sandia.gov (V.S. Neary).

1364-0321/$ - see front matter Published by Elsevier Ltd.
http://dx.doi.org/10.1016/j.rser.2013.05.033

and

$$\overline{P} = \frac{1}{2} \times a \times \rho \times \overline{u^3} = \frac{1}{2} \times a \times \rho \times (1 + 3I_u^2 + \gamma I_u^3) \times \overline{u}^3 \quad (2)$$

where ρ is the fluid density, a is the ECA, u is the instantaneous horizontal current velocity component, and $\gamma = \overline{u'^3}/\sigma^3$ is the skewness coefficient (which is negligible). The instantaneous horizontal current velocity component is assumed to be the predominant velocity component, which is perpendicular to the ECA at all times and is defined as the sum of the mean velocity and velocity fluctuation

$$u = \overline{u} + u' \quad (3)$$

The turbulence intensity is defined as

$$I_u = \sigma_u/\overline{u} \quad (4)$$

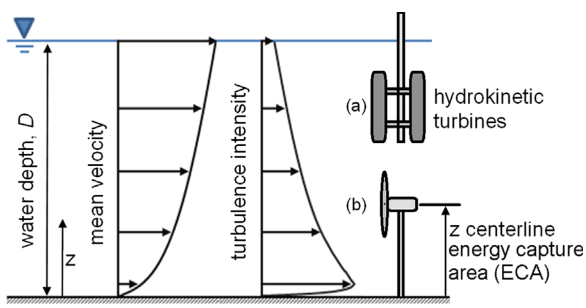


Fig. 1. Typical profiles of velocity and turbulence intensity in an open channel flow. The figure illustrates two possible hydrokinetic turbine configurations: a surface deployed vertical axis turbine (a) and a bottom deployed tower-mounted horizontal-axis turbine (b).

where $\sigma_u = \sqrt{\overline{u'u'}}$ is the standard deviation or root-mean-square (RMS) velocity. Detailed derivations of Eqs. (1) and (2) are provided in Appendix 1. These equations show that accurate assessment of the average hydrodynamic force and available power requires resolution of the turbulent fluctuations and turbulence intensity as well as the mean velocity. For example, a turbulence intensity equal to 20% at hub height of the CEC machine can increase the hydrodynamic force and power by 4% and 12.8%, respectively. The effects of turbulence should therefore be considered in the structural design and energy production calculations of a CEC machine.

In medium to large rivers that are desirable sites for commercial scale CEC development, defined here as open-channel flows with 50th percentile depths that exceed one meter and 50th percentile currents greater than 1 m/s, collecting accurate measurements of the instantaneous velocity u needed to calculate basic inflow metrics (such as $\overline{u}$, I_u, $\overline{F}$, and $\overline{P}$) is challenging [1]. River flows also exhibit great temporal variability of discharge and depth over time scales varying from minutes to days. For example, the USGS gage data for daily discharge and stage on the Missouri River, illustrated in Fig. 2, shows that discharges and water stages can increase tenfold during extreme episodic flood events over an approximately thirty-year period. This large variability in river discharge and depth is commonly observed and will affect the magnitude and distribution of mean velocity and turbulence over the ECA of a CEC machine over its design life. However, profile measurements needed to obtain meaningful statistics on the spatiotemporal variability of such important inflow metrics would rarely if ever be available due to the high cost and difficulty in obtaining such measurements. To obtain such measurements, an acoustic Doppler current profiler (ADCP) is the most practical and

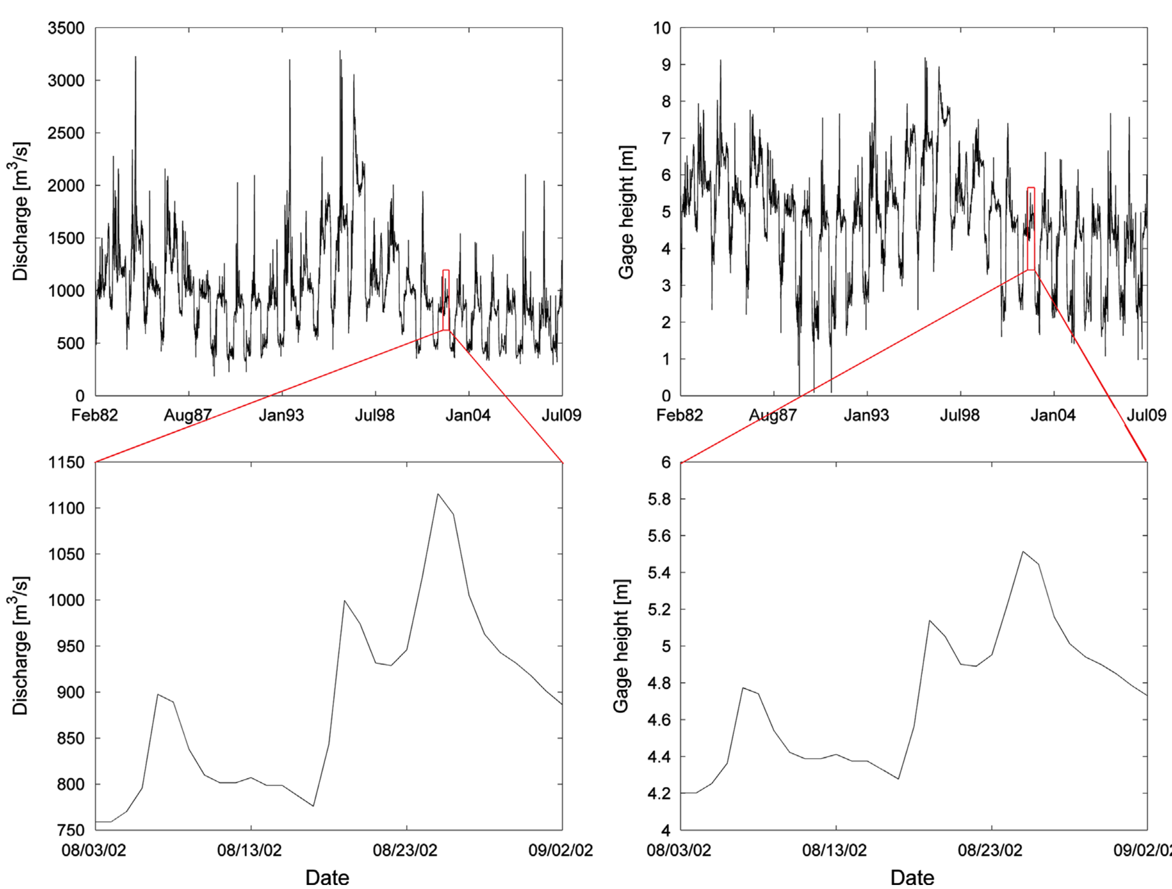


Fig. 2. Daily flow and gage height time-series record for approximately thirty-year period of record (POR) on the Missouri River, Nebraska (USGS 06610000). The inset plots show the flow and gage height time series during field measurements by Holmes and Garcia (2009).

economical instrument to measure the vertical profile of $\overline{u}$ at a given site. But unlike an acoustic Doppler velocimeter (ADV), an ADCP typically cannot resolve the higher frequency turbulence in the inertial subrange and exhibits greater instrument noise [2–4]; therefore, ADCPs usually cannot provide an accurate estimate of the turbulence intensity I_u.

Alternatively, mean velocity and turbulence profiles in rivers may be simulated using numerical or analytical models. Analytical models include simple power and logarithmic laws for the vertical profiles of mean velocity for a flat plate turbulent boundary layer flow [5] and exponential decay models developed by Nezu and Nakagawa [6] for profiles of the longitudinal (predominant), transverse, and vertical root-mean-square velocities, $\sqrt{\overline{u'u'}}$, $\sqrt{\overline{v'v'}}$, and $\sqrt{\overline{w'w'}}$, respectively. An evaluation of flat plate boundary layer models by Nezu and Nakagawa [6], who compared model predictions of turbulence profiles with measurements from large rivers and canals reported by McQuivey [7], suggests that these models can perform reasonably well despite simplifying assumptions of steady uniform flow with fully-developed boundary layers. These assumptions are generally violated for most river flows where the channel geometry, roughness, mean-section depth, and bulk velocity typically vary along the longitudinal direction. River currents are often three-dimensional as a result of variations in river alignment and vortices forming at different length scales from bed forms and in-stream structures [8], e.g. bridge piers. Pressure gradients associated with nonuniform surface profiles and bed forms, including ripples, dunes and anti-dunes, and wind shear can cause significant departures from semi-theoretical models that estimate mean and root-mean-square velocity profiles [9,10]. Nevertheless, the simple analytical models can be useful for obtaining first order approximations of inflow characteristics at a CEC site.

In this study, our aim is to examine measured vertical profiles of velocity and turbulence in open channel flows to:

(1) Assess the validity of classical models for predicting river inflow characteristics along a planned ECA of a CEC machine.
(2) Determine the range of velocities and longitudinal turbulence intensities that CEC technologies may be exposed to over their design life as a result of the large variation of water depth typical for river flows.

2. Methods

While ADCP measurements in medium and large rivers are now reported with increasing regularity in the literature, data is usually limited to mean velocity measurements only, e.g. [11], [12]. This present study examines previously reported vertical profiles of predominant RMS velocity measurements (i.e. turbulence) as well as mean velocity. Published profiles from five rivers [7,13,15,16], a large water supply canal [7], and a laboratory flume [7] were examined. Aside from the flume measurements we limited our literature review to open channel flows which meet our criteria for “medium to large rivers” as described in Section 1 since these are the sizes of channels which provide the most interest to CEC developers. The ranges of bulk flow properties reported during data collection, including discharge Q, water profile depth D, and section width W, are summarized in Table 1. Three of the rivers had depths of at least two meters with velocities exceeding 1 m/s at the time of measurement. For several sites, mean annual discharge Q_m records were available to compare with discharges reported during the time of measurements. All Reynolds numbers R were above 4×10^5. Froude numbers F for all cases indicate subcritical flows with the largest F observed for the Hurunui River [15].

In order to derive a shear velocity from the reported field measurements, the longitudinal velocity profiles were compared with the log-law [6], which describes the vertical distribution of longitudinal velocity in open channel flows with rough boundaries,

$$\frac{\overline{u}}{u_*} = \frac{1}{\kappa}\ln\left(\frac{z}{k_s}\right) + 8.5 \quad (5)$$

We computed the shear velocity $u_* = \sqrt{\tau_o/\rho}$ from the slope of the best fit line through the time averaged velocity profile. With the exception of the Holmes & Garcia [13] data set, many of the vertical profiles contained only one or two data points in the wall region ($z/D<0.2$) where the log law applies. For these cases, data from the entire vertical profile was used in this fitting method to calculate the shear velocity. Results for shear velocity using this method compared well with the values reported by the original investigators. Profiles with significant non-monotonic behavior, due to 3D flow effects or vortex shedding, were eliminated. This non-monotonic behavior was identified when the fitting procedure for the shear velocity resulted in a poor coefficient of determination, R^2. Any profiles with R^2 values less than 0.8 were discarded. Of the velocity profiles reviewed, only 12% were eliminated because they exhibited non-monotonic behavior or could not be well represented by the log law. The final dataset included 47 profiles.

Measured profiles of $\overline{u}$ non-dimensionalized $\overline{u}_{\max}$ by were plotted to compare with the power law equation used for fully

Table 1
Bulk flow properties of reviewed open channel flow data.

Investigators	Site	Q_m (m^3/s)	Q^d (m^3/s)	D^d (m)	W^d (m)	Re^e (10^6)	Fr^e
McQuivey [6]	Mississippi	19000[a]	7900–9200	7.4–16	570–890	3–9	0.06–0.17
McQuivey [6]	Missouri	910[b]	890–920	2.9–3.1	200–210	4–38	0.19–0.35
Holmes & Garcia [12]	Missouri	2200[c]	1400	4.9	350–400	5–9	0.13–0.17
McQuivey [6]	Rio Grande canal	NR	14–26	0.85–0.91	21–22	0.8–1.3	0.36–0.49
Nikora & Smart [14]	Hurunui	NR	250	1.1–1.2	85–90	1–5	0.70–0.79
Carling et al. [10]	Severn	NR	100	NR	NR	3–6	0.10–0.16
McQuivey [6]	2.44 m flume	NR	1–2	0.33-0.53	2.44	0.4–0.8	0.69-0.74
Gunawan et al. [15]	Blackwater	NR	1.87–3.57	0.65-0.97	5.74-6.75	0.2–0.3	0.14–0.19

NR = not reported.
[a] Mean annual discharge from nearest USGS station #07289000, record period: 2009.
[b] Mean annual discharge from nearest USGS station #06610000, record period: 1953–2009.
[c] Mean annual discharge from nearest USGS station #06935965, record period: 2001–2010.
[d] Reported by original investigators at time of measurement.
[e] Derived by authors, using depth averaged velocity and local water depth.

developed flat plate boundary layer flows

$$\frac{\bar{u}}{\bar{u}_{\max}} = \left(\frac{z}{D}\right)^{1/a} \quad (6)$$

and to determine the fitted power law exponent $1/a$. The derivation in Appendix 2, shows that a value of $\alpha = 6$ is consistent with the Manning's equation.

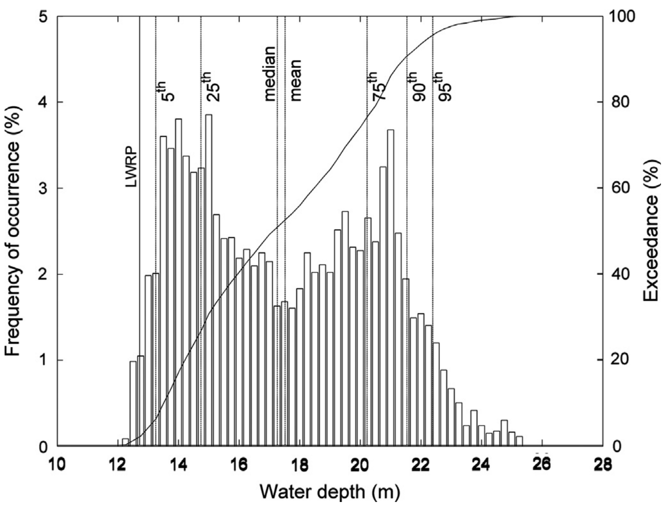


Fig. 3. Histogram of water depths at a planned turbine deployment site at the Mississippi river near Baton Rouge, LA.

Similarly, measured profiles of RMS velocities normalized by the shear velocity $u_* = \sqrt{\tau_o/\rho}$ were plotted to evaluate the accuracy of the exponential decay models developed by Nezu and Nakagawa [6] for steady uniform flow in smooth laboratory flumes

$$\sqrt{\overline{u'u'}}/u_* = 2.30\exp(-z/D) \quad (7a)$$

$$\sqrt{\overline{v'v'}}/u_* = 1.63\exp(-z/D) \quad (7b)$$

$$\sqrt{\overline{w'w'}}/u_* = 1.27\exp(-z/D) \quad (7c)$$

These expressions, Eq. (7a)–(7c), are universal for smooth boundaries between (0.1 and 0.2) $< z/D < 0.9$, independent of Reynolds and Froude numbers, and show that $\sqrt{\overline{u'u'}}/u_* > \sqrt{\overline{v'v'}}/u_* > \sqrt{\overline{w'w'}}/u_*$. They do not apply near the wall, approximately $z/D <$ (0.1 to 0.2), as the no-slip condition requires turbulence intensities to decrease from a maximum value to zero at $z/D = 0$. Nor do these equations apply in the free surface region above $z/D < 0.9$, where $\sqrt{\overline{w'w'}}/u_*$ is dampened.

To demonstrate how to evaluate the spatiotemporal variability of mean velocity and turbulence acting on the ECA of a CEC machine, we performed a case study based upon conditions at Scotlandville Bend, Mississippi River near Baton Rouge, LA. This location is the site of a planned commercial river energy project by Free Flow Power (FFP) LLC, and was the basis for the river current hydrokinetic resource reference model proposed by Sandia National Laboratories [17]. This hydrokinetic resource reference

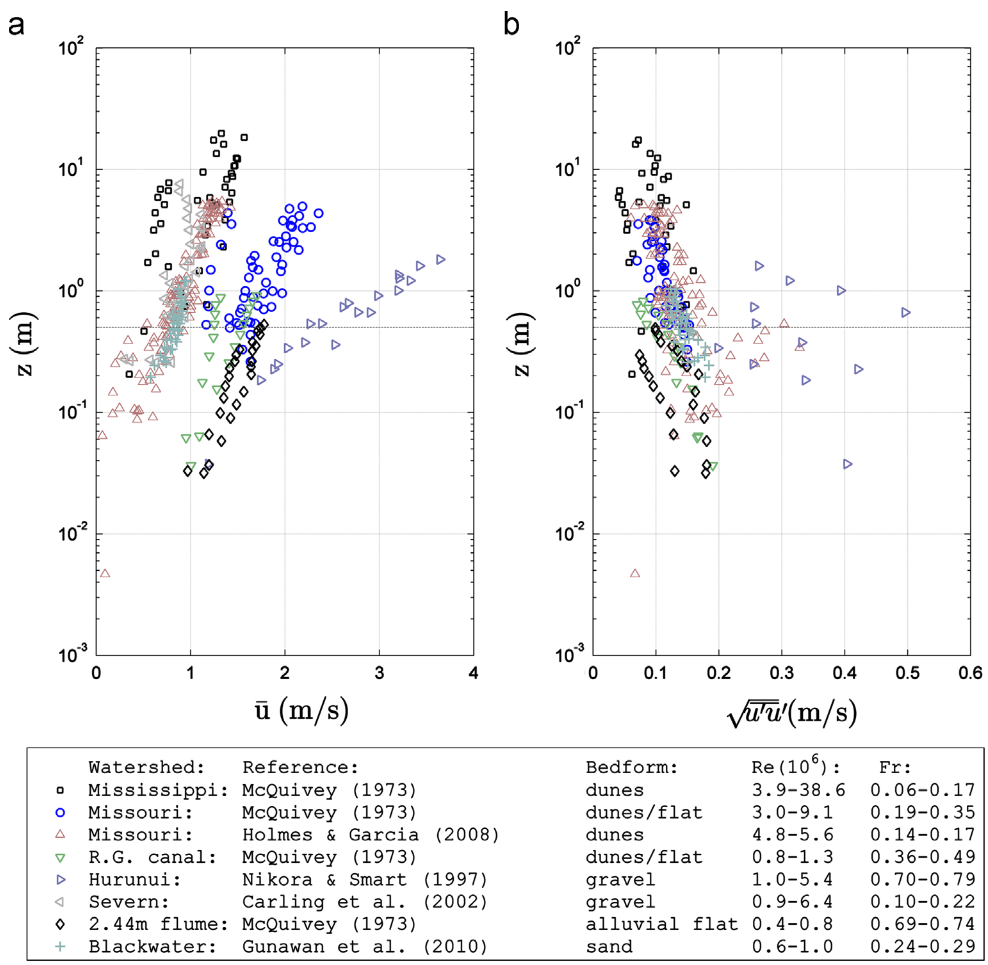


Fig. 4. (a) Mean longitudinal velocity profiles. (b) Longitudinal RMS velocity profiles. The dashed horizontal line indicates $z = 0.5$ m. CEC technologies will operate at depths greater than 0.5 m off the bed.

model included an idealized trapezoidal river cross-section based on river transects with the low water reference plane (LWRP) at 1.2 m NAVD (North American Vertical Datum), channel bottom at −11.5 m NAVD, and top of bank at 18.5 m NAVD. The FFP turbines are ducted axial-flow turbines that are three meters in diameter (d), which can be deployed from towers mounted to the river bottom or pontoons at the water surface. Although the US Coast Guard requires that the turbines be deployed at this site 6.1 m below the LWRP so as not to pose a hazard to river navigation, we performed our analysis neglecting this constraint—making this work applicable to other CEC technologies at possibly different sites where deployment depth restrictions may not apply.

The variation of the mean velocity and turbulence acting on the ECA is examined at low and high water depths for two deployment scenarios: a turbine deployed from a tower with the rotor hub 1.5d above the river bed, and a turbine deployed from a pontoon with the rotor hub 1.5d below the water surface. Based on water stage measurements over a 25-year period of record from the nearest U.S. Army Corps of Engineers' gage, located 8 km downstream of the site, the low water depth is defined for the purpose of this study as the 25th percentile value ($D=14.74$ m) and high water depth is defined as the 90th percentile value ($D=21.54$ m). The LWRP, at 12.7 m, is the 2nd percentile water depth. The results of the statistical analysis of water depth are summarized in the frequency and cumulative frequency histograms shown in Fig. 3.

3. Results and discussion

All mean longitudinal velocity $\overline{u}$ profiles and RMS velocities are plotted in Fig. 4a and b, with the elevation above the bed z plotted on the logarithmic scale to accentuate the spread of depth and velocity in the data examined. We assume that $z=0.5$ m above the bed is a conservative lower limit on the location of the lower boundary of the ECA. Positioning the ECA closer to the bed would cause undesirable effects, including reducing the available power that can be harvested in the water column, increasing hydrodynamic load asymmetries and turbulence levels, and increasing the risk of strike or fouling by sediments or mobile bedforms. The mean currents $\overline{u}$ are observed to equal or exceed 0.5 m/s, with maximum velocities near the water surface and generally ranging from 1 to 3.7 m/s. Given that flow measurements for the Mississippi River by McQuivey [7] were taken when the flow was well below the mean annual discharge Q_m (Table 1), one would expect higher maximum $\overline{u}$ at higher z for flows with $Q>Q_m$. The corresponding longitudinal RMS velocity profiles, shown in Fig. 4b, increase exponentially from the free water surface to the near wall region. For fixed beds, the no-slip condition requires that the turbulence intensity and all components of the Reynolds stress tensor are zero at the bed, but rivers typically have mobile beds with a non-zero mean velocity and Reynolds stresses. The RMS velocities $\sqrt{\overline{u'u'}}$ are observed to range between 0.04 m/s and 0.5 m/s. At high currents, such as the River Hurunui, which has a maximum velocity of nearly 4 m/s, the RMS velocity $\sqrt{\overline{u'u'}}$ is at a maximum of 0.5 m/s. Values of $\sqrt{\overline{u'u'}}$ for the Holmes and Garcia [13] data are noteworthy because they are quite high with respect to their mean velocity values.

Longitudinal turbulence intensity I_u profiles with z normalized by the flow depth D are shown in Fig. 5, and the root-mean-square velocity $\sqrt{\overline{u'u'}}$ is plotted on a logarithmic scale to show the large variation of turbulence. The plot shows that the maximum values of I_u typically occur very close to the bed. The longitudinal turbulence intensity I_u increases exponentially from the free water surface $z/D=1$ into the near wall region $z/D<0.1$, but the large scatter indicates that $\sqrt{\overline{u'u'}}$ does not scale well with $\overline{u}$.

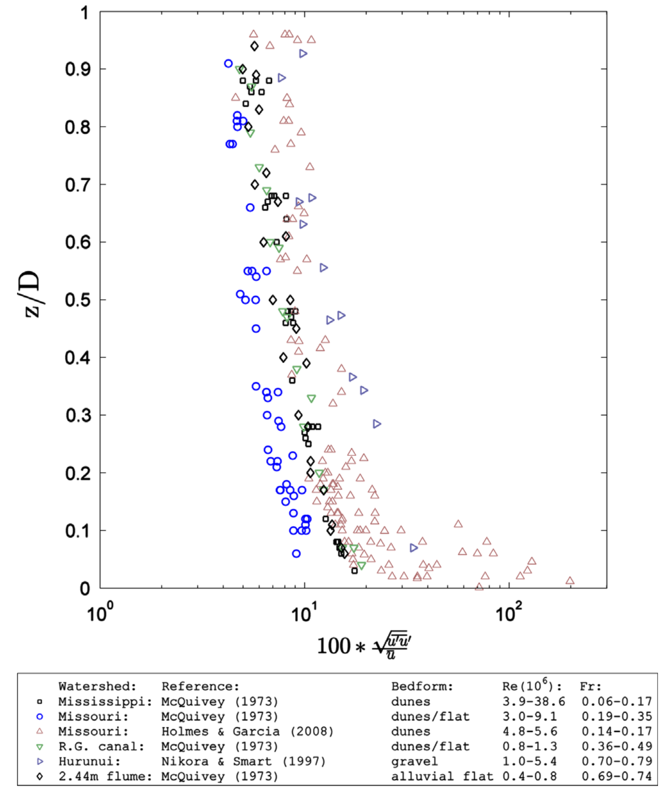


Fig. 5. Longitudinal turbulence intensity profiles with z normalized by the flow depth and the turbulence intensity normalized by the local mean velocity and multiplied by 100 to determine the percentage of turbulence intensity with respect to the local mean velocity.

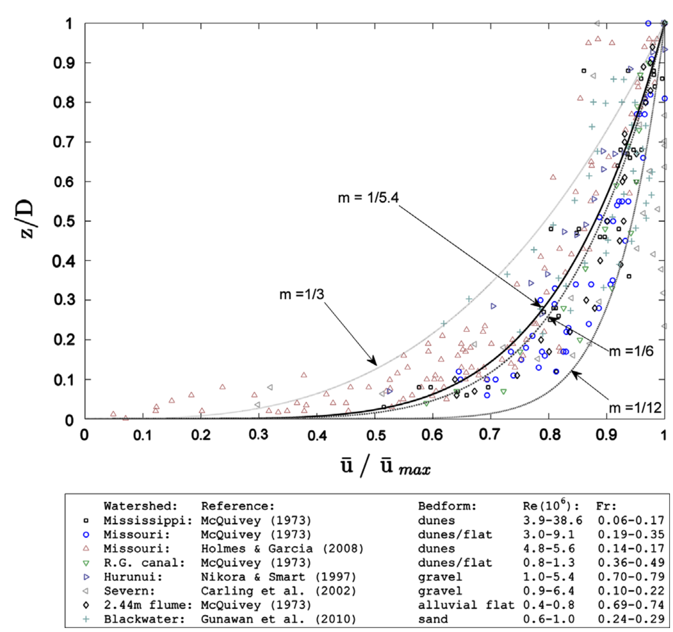


Fig. 6. Power law velocity profiles with z normalized by D and $\overline{u}$ normalized by $\overline{u}_{max}$. The solid black line represents the best fit of the power law with exponent $1/\alpha$ through the data, and the resulting best fit $\alpha=5.4$ ($R^2=0.999$). The grey lines (left to right) represent the power law with exponent 1/3, 1/6 and 1/12, respectively.

Field measurements of $\overline{u}$ non-dimensionalized by $\overline{u}_{max}$ are compared with the power law Eq. (6) in Fig. 6. Based on the power law assumption, $\overline{u}_{max}$ occurs at the surface ($z/D=1$), but the

measured data shows that $\bar{u}_{max}$ can occur beneath the surface due to wind, wave and three-dimensional flow effects. The power law exponent $1/a$ was observed to vary from 1/3 to 1/12 between individual profiles, with a best fit value of 1/5.4 through all the data, which is in good agreement with the theoretical value 1/6 that was shown to be consistent with the Manning's equation (Appendix 2). Variation in the exponent can be attributed to a number of causes, including measurement error, pressure gradients, roughness and three-dimensional flow effects.

Field measurements of normal stresses, e.g. $\sqrt{u'u'}$, normalized by shear velocity $u_* = \sqrt{\tau_0/\rho}$ with exponential decay models developed by Nezu and Nakagawa [6] are compared in Fig. 7. The value of $\sqrt{u'u'}/u_*$ is expected to reach maximum near the bed, then gradually decreasing to zero at the wall (bed) [14]. A peak value of $\sqrt{u'u'}/u_*$=3.8 was observed in the near-wall region by Holmes and Garcia [6]. This large departure from the exponential decay model may have been due to turbulence generated by the presence of dunes. The gradual decrease to zero, however, cannot be observed because of lack of measurements close to the bed. Obtaining such data is difficult in the field because of limitations inherent in the instrument used for measurements. Field measurements are in reasonable agreement with the exponential

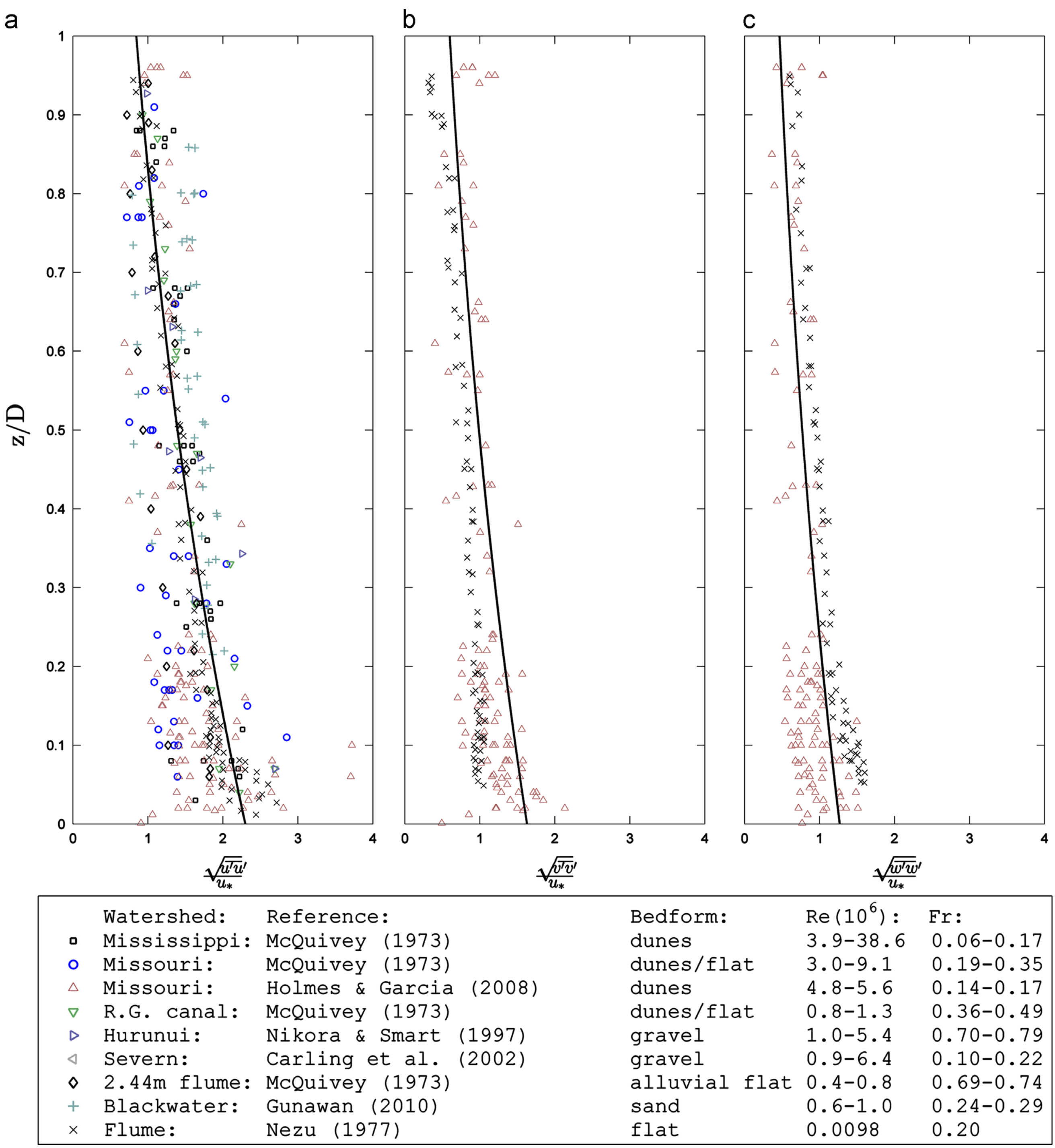


Fig. 7. Exponential decay law profiles by Nezu and Nakagawa (1993) compared to field measurements, with z normalized by D and normal stresses, e.g. $\sqrt{u'u'}$ normalized by shear velocity $u_* = \sqrt{\tau_0/\rho}$.

decay models developed from laboratory flumes, although there is considerable scatter; likely due to a combination of measurement error and complex hydrodynamic effects summarized previously. The measurements by Holmes and Garcia [13] are the only measurements known by the authors to include normal Reynolds stresses $\sqrt{\overline{v'v'}}/u_*$ and $\sqrt{\overline{w'w'}}/u_*$ in large rivers (depths >1 m and currents >1 m/s). These turbulence measurements are in fair agreement with the exponential decay models, except near the surface where the models underestimate the data. The discrepancies can be attributed to measurement errors due to wave motion, wind shear effects, or close proximity of the measurement sample volume from the measurement boat.

The effect of river depth (D) variation on the vertical location and size of the ECA relative to the characteristic profiles for the velocity and turbulence is shown in Fig. 8 for the geometry and flow properties described for the Scotlandville Bend site (Section 2). The location and height of the ECA, like the mean velocity and turbulence profiles, are non-dimensionalized by the water depth D, which results in variation of the *relative* location and height of the ECA with water depth. This non-dimensionalization allows a comparison of the relative location and relative size of the ECA for extreme low and high water depth over the velocity and turbulence profiles for the near-bed and near-surface deployment scenarios. Furthermore, one can apply the power law (Eq. (6) with an exponent $1/a=1/6$) and the exponential decay model for the longitudinal turbulence intensity (Eq. (7a)) to quantify the effect of depth variation on the inflow metrics $\overline{u}$, I_u, $\overline{F}$, and $\overline{P}$ between the low and high depth extremes—values for these inflow metrics based upon this methodology are given in Table 2.

River depth variability will adjust the relative location and length of the ECA at the low and high water depth extremes as shown in Fig. 8 for the two deployment scenarios considered. The high depth in this example is 46% greater than the low depth. The depth-averaged velocity U and maximum surface velocities $\overline{u}_{\max}$ (based on rating curves provided for the USACE gage site) are greater by 85% at the high depth compared to the low depth (Table 2). For the near-bed deployment scenario, the turbine hub height moves downward by $0.1(z/D)$ from the low and high water extremes. Application of the power law indicates that the mean velocity $\overline{u}$ at hub height (i.e. centerline of ECA) increases by 72%, the turbulence intensity I_u (Eq. (4)) at hub height drops by 38%, the hydrodynamic force increases by 193%, and the available power increases by 373%. Minimum and maximum values of these parameters (at each end of the ECA), and percent differences between these values at the low and high depths, are also provided. For the near-surface deployment scenario, the turbine hub height moves upward by $0.1(z/D)$ from the low and high water extremes (Table 2). The mean velocity $\overline{u}$ at hub height increases by 89%, the turbulence intensity I_u (Eq. (4)) at hub height drops by 29%, the hydrodynamic force increases by 241%, and the available power increases by 493%.

Decreases in turbulence intensity can be deceptive because it is normalized by the local mean velocity. Gunawan et al. [18] showed that turbulence at a hydrokinetic energy site increases with mean velocities, while at the same time turbulence intensities decreases. In both near-surface and bottom deployment scenarios, observed reductions in turbulence intensity $I_u=\sigma_u/\overline{u}$ actually result in increases in the turbulence. For the near-surface deployment scenarios at hub-height, while I_u drops by 29% between cases 2a and 2b, turbulence actually increases by 37% (Table 2). Similarly for the bottom deployment scenarios at hub-height, while I_u drops from 0.24 to 0.15 between cases 1a and 1b, turbulence actually increases by 5% from 0.21 to 0.22. This observation implies that fatigue load increases with mean velocities while at the same time turbulence intensities decreases.

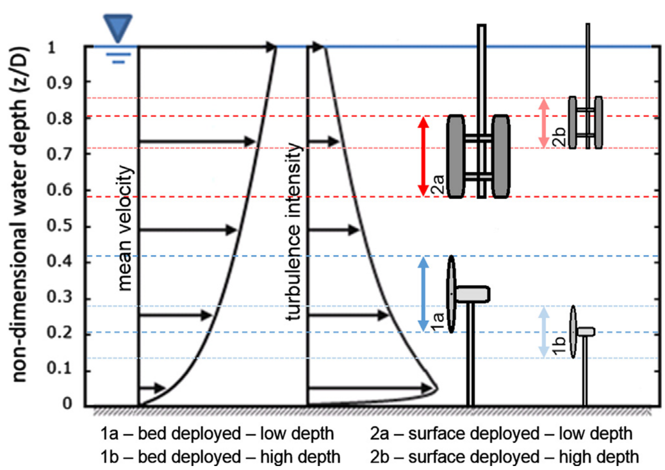


Fig. 8. Effects of large depth variability on the location of the swept area (energy capture area) relative to the velocity and turbulence profiles.

4. Conclusions

Accounting for the reduced accuracy of velocity and turbulence measurements in large rivers and the uncertainty in calculation of the shear velocity, the power law (Eq. (6)) and exponential decay model (Eq. (7a)–(7c)) reasonably approximated the average distribution of the local velocity and turbulence measurements reviewed. The results suggest that these models can be used for first-order approximations of the spatiotemporal variations of river inflow parameters arising from large depth variations, which can then be used to predict hydrodynamic forces and available power that a CEC will experience over its design lifetime. The scatter does indicate that more accurate estimates of velocity and turbulence will require advanced numerical modeling supported by site measurements of mean velocity and turbulence profiles. More field measurements in rivers using acoustic Doppler current profilers (ADCP) and acoustic Doppler velocimeters (ADV) are needed to expand the limited data presently available for large

Table 2
First order approximation of extreme river depth variation on inflow characteristics relevant to CEC machines at river hydrokinetic resource reference site.

Case	D (m)	z_{hub}/D (−)	U (m/s)	u_{max} (m/s)	$\overline{u}$ (m/s)			σ_u (m/s)			I_u (−)			$\overline{F}$ (kN)	$\overline{P}$ (kW)
					Min	Max	hub	Min	Max	hub	Min	Max	hub		
1a	14.74	0.31	0.92	1.04	0.8	0.9	0.86	0.21	0.21	0.21	0.26	0.23	0.24	2.7	2.6
1b	21.54	0.21	1.7	1.92	1.38	1.55	1.48	0.22	0.23	0.22	0.16	0.15	0.15	7.9	12.3
Δ%	46	−32	85	85	71	73	71	6	12	8	−35	−35	−36	188	371
2a	14.74	0.69	0.92	1.04	0.96	1	0.98	0.31	0.30	0.30	0.32	0.3	0.31	3.7	4.3
2b	21.54	0.79	1.7	1.92	1.82	1.87	1.85	0.40	0.41	0.41	0.22	0.22	0.22	12.6	25.5
Δ%	46	14	85	85	91	87	90	30	37	34	−31	−27	−29	238	500

1a. Bottom deployed low depth, 1b. Bottom deployed high depth, 2a. Surface deployed low depth, 2b. Surface deployed high depth.

rivers with fast currents. With limited site data, including a gage station with a daily or hourly water stage record, a stage-discharge rating curve, and a stage-area rating curve, we demonstrate how to apply these simple models to derive first-order approximations of the spatiotemporal variation of velocity and turbulence over the ECA of a CEC at a given river hydrokinetic energy site if three-dimensional effects are minimal, the channel is sufficiently wide, and the exponent for the power velocity law is reasonably accurate. The depth-averaged velocity U can be approximated using the equation in Appendix 2, the maximum velocity for the power law calculated as $\overline{u}_{\max}=(7/6)U$ (Appendix 2), and the shear velocity $u_*=\sqrt{gDS}$.

A case study was performed to demonstrate the effects of extreme depth variation on velocity and turbulence profiles for a three-meter diameter ducted axial flow turbine at a river hydrokinetic resource reference site, using the power law (with its exponent set to be consistent with the Manning's equation) and an exponential decay model. The analysis showed pronounced changes to $\overline{u}$, I_u, $\overline{F}$, and $\overline{P}$ between the low and high water depth extremes, which highlights the importance of modeling these spatiotemporal effects at river hydrokinetic energy sites. Significant engineering implications on CEC machine structural loads, annual energy production, and cost of energy arise due to these variations in the mean velocity, turbulence intensity, hydrodynamic force, and available power over the ECA.

Notation

a	energy capture area (m^2)
α	denominator in power law exponent (−)
d	turbine diameter (m)
D	flow depth (m)
F	Froude Number (−)
$\overline{F}$	time-averaged hydrodynamic force (N)
γ	skewness coefficient (−)
I_u	turbulence intensity of the streamwise velocity component (−)
κ	von Karman constant (−)
k_s	roughness height (m)
m	$1/\alpha$, power law exponent (−)
$\overline{P}$	time-averaged power (W)
Q	discharge (m^{-3}/s)
Q_m	mean annual discharge (m^{-3}/s)
R	Reynolds Number (−)
ρ	fluid density (kg/m^3)
σ_u	standard deviation or root-mean-square velocity (m/s)
τ_o	boundary shear stress (N/m^2)
U	depth-averaged velocity (m/s)
u, v, w	instantaneous longitudinal, lateral and vertical velocity (m/s)
$\overline{u}$	local time-averaged longitudinal velocity (m/s)
$\overline{u}_{\max}$	maximum time-averaged longitudinal velocity (m/s)
u', v', w'	instantaneous longitudinal, lateral and vertical velocity fluctuation (m/s)
u_*	shear velocity (m/s)
ν	kinematic viscosity (m^2/s)
W	river width (m)
z	height above channel bed (m)

Acknowledgments

This research was supported by the U.S. Department of Energy's (DOE) Office of Energy Efficiency and Renewable Energy, Wind and Water Power Technologies Program. Oak Ridge National Laboratory is managed by UT-Battelle, LLC for DOE under contract DE-AC05-00OR22725. We thank Bob Holmes of the United States Geological Survey for providing velocity and turbulence measurement data he collected on the Missouri River, and Ed Lovelace of Free Flow Power, LLC, who provided information on turbine design locations at the Scotlandville Bend, Mississippi River site. Discussions with Leonardo P. Chamorro, assistant professor at the University of Illinois, motivated the detailed derivations in Appendix 1. The final result is well known in the wind energy research community, but we were unable to find any published derivation to cite.

Appendix 1. Derivation of Reynolds averaged hydrodynamic force and power

For hydrodynamic force calculation in Eq. (1), using Reynolds decomposition, u^2 can be expressed as follows:

$$u^2=(\overline{u}+u')^2$$
$$u^2=(\overline{u}+u')(\overline{u}+u')$$
$$u^2=\overline{u}^2+2\overline{u}u'+u'^2$$
$$\overline{u^2}=\overline{\overline{u}^2}+\overline{2\overline{u}u'}+\overline{u'^2}$$
$$\overline{u^2}=\overline{u}^2+\overline{u'^2}$$
$$\overline{u^2}=\left(1+\frac{\overline{u'^2}}{\overline{u}^2}\right)\overline{u}^2$$
$$\overline{u^2}=(1+I_u^2)\overline{u}^2$$

Therefore the power includes an additional term that is proportional to the turbulence intensity squared.

For available power calculation in Eq. (2), using Reynolds decomposition, u^3 can be expressed as follows:

$$u^3=(\overline{u}+u')^3$$
$$u^3=(\overline{u}+u')^2(\overline{u}+u')$$
$$u^3=(\overline{u}^2+2\overline{u}u'+u'^2)(\overline{u}+u')$$
$$u^3=\overline{u}^3+\overline{u}^2u'+2\overline{u}^2u'+2\overline{u}u'^2+\overline{u}u'^2+u'^3$$
$$u^3=\overline{u}^3+3\overline{u}^2u'+3\overline{u}u'^2+u'^3$$
$$\overline{u^3}=\overline{\overline{u}^3}+\overline{3\overline{u}^2u'}+\overline{3\overline{u}u'^2}+\overline{u'^3}$$
$$\overline{u^3}=\overline{u}^3+3\overline{u}\overline{u'^2}+\overline{u'^3}$$
$$\overline{u^3}=\left(1+3\frac{\overline{u}}{\overline{u}}\frac{\overline{u'^2}}{\overline{u}^2}+\frac{\overline{u'^3}}{\overline{u}^3}\right)\overline{u}^3$$
$$\overline{u^3}=\left(1+3\frac{\overline{u'^2}}{\overline{u}^2}+\frac{\overline{u'^3}}{\overline{u}^3}\frac{\sigma^3}{\sigma^3}\right)\overline{u}^3$$
$$\overline{u^3}=(1+3I_u^2+\gamma I_u^3)\overline{u}^3$$

where skewness, $\gamma=\overline{u'^3/\sigma^3}$.

Appendix 2. Derivation of Power Law Exponent consistent with the Manning's Equation

Given the power-law vertical mean velocity distribution in a very wide open channel:

$$\frac{\overline{u}}{u_*}=a\left(\frac{z}{k_s}\right)^{1/a}$$

where $\overline{u}$ is the local mean velocity; u_* is the shear velocity; a is a constant; z is the distance above the channel bed; k_s is the equivalent sand-grain roughness; and $1/a$ is the exponent.

Integrate the point velocity distribution to find the mean velocity:

$$U=\frac{1}{D}\int_0^D au_*\left(\frac{z}{k_s}\right)^{1/a}dz=\frac{au_*}{(1/\alpha+1)D}\left(\frac{D}{k_s}\right)^{1/a+1}k_s$$

$$U=\frac{au_*}{(1/a+1)}\left(\frac{D}{k_s}\right)^{1/a}$$

The maximum velocity occurs at $z=D$, and is given by

$$\overline{u}_{\max}=au_*\left(\frac{D}{k_s}\right)^{1/a}$$

Therefore,

$$\frac{\overline{u}}{\overline{u}_{\max}}=\left(\frac{z}{D}\right)^{1/a}$$

Comparing the expressions for U and $\overline{u}_{\max}$, we have

$$U=\frac{\overline{u}_{\max}}{1/a+1}$$

Rewrite the expression for mean velocity, substituting $u_*=\sqrt{gDS}$, to obtain

$$U=\frac{a\sqrt{g}}{(1/a+1)k_s^{1/a}}D^{1/a+1/2}S^{1/2}$$

With a value $\alpha=6$, this equation for U agrees with Manning's and Strickler's equations in the exponents on D, k_s, and S. The Manning's equation is therefore compatible with a 1/6 power law velocity distribution, and the maximum velocity at the surface can be related to the depth-averaged velocity U by the expression, $\overline{u}_{\max}=(7/6)U$.

References

[1] Neary VS, Gunawan B, Polagye B, Thomson J, Richmond MC, Durgesh V, Muste M M, Fontaine A. Field measurements at river and tidal current sites for hydrokinetic energy development: best practices manual. ORNL/TML-2011/419 2011.
[2] Stone MC, Hotchkiss RH. Evaluating velocity measurement techniques in shallow streams. Journal of Hydraulic Research, IAHR 2007;45(No. 6):752–62.
[3] Gunawan B, Sterling M, Knight DW. Using an acoustic Doppler current profiler in a small river. Water and Environment Journal 2010;24(no. 2):147–58.
[4] Thomson J, Polagye B, Durgesh V, Richmond MC. Measurements of turbulence at two tidal energy sites in Puget Sound, WA. IEEE Journal of Oceanic Engineering 2012;37(No. 3).
[5] White FM. Viscous fluid flow. McGaw-Hill; 1974.
[6] Nezu I, Nakagawa. H. Turbulence in open-channel flows. IAHR Monograph Series. Rotterdam: A. A. Balkema; 1993.
[7] McQuivey RS. Summary of turbulence data from rivers, conveyance channels, and laboratory flumes. USGS Report 802-B turbulence in water, 1973.
[8] Shiono K, Knight DW. Turbulent open-channel flows with variable depth across the channel. Journal of Fluid Mechanics. . Cambridge University Press; 617–646.
[9] Lyn DA. Turbulence measurements in open-channel flows over artificial bed forms. Journal of Hydraulic Engineering-ASCE 1993;119(3):306–26.
[10] Song T, Chiew YM. Turbulence measurement in nonuniform open-channel flow using acoustic Doppler velocimeter (ADV). Journal of Engineering Mechanics-ASCE 2001;127(3):219–32.
[11] Carling PA, Cao Z, Holland MJ, Ervine DA, Babaeyan-Koopaei K. Turbulent flow across a natural compound channel. Water Resources Research 2002;38(12):1270.
[12] Clarke RT. Hydrological prediction in a non-stationary world. Hydrology and Earth System Sciences 2007;11(1):408–14.
[13] Holmes RR, Garcia MH. Flow over bedforms in a large sand-bed river: a field investigation. Journal of Hydraulic Research 2008;46(3):322–33.
[14] Kironoto BA, Graf WH. Turbulence characteristics in rough non-uniform open-channel flow. Proceedings of the Institution of Civil Engineers-Water Maritime and Energy 1995;112(4):336–48.
[15] Nikora VI, Smart GM. Turbulence characteristics of New Zealand gravel-bed rivers. Journal of Hydraulic Engineering 1997;123(9):764–73.
[16] Gunawan B, Sun X, Sterling M, Shiono K, Tsubaki R, Rameshwaran P, Knight DW, Chandler J, Tang X, Fujita. I. The application of LS-PIV to a small irregular river for inbank and overbank flows. Flow Measurement and Instrumentation April 2012;24:1–12.
[17] Previsic M, Jepsen R. Design, performance, and economic assessment for reference models 1 and 2, O.o.E.E.a.R.E. US Department of Energy, Water Power Program. Sandia National Laboratory; 100.
[18] Gunawan B, Neary VS, Colby J. Mean velocity and turbulence measurements at a tidal energy site in East River, NY (USA). Under review, Renewable Energy.